Journal of Power Sources 215 (2012) 36–42

Contents lists available at SciVerse ScienceDirect

Journal of Power Sources

journal homepage: www.elsevier.com/locate/jpowsour

Hierarchical composites of sulfonated graphene-supported vertically aligned polyaniline nanorods for high-performance supercapacitors

Biao Ma, Xiao Zhou, Hua Bao, Xingwei Li, Gengchao Wang*

Key Laboratory for Ultrafine Materials of Ministry of Education, Shanghai Key Laboratory of Advanced Polymeric Materials, School of Materials Science and Engineering, East China University of Science and Technology, Shanghai 200237, PR China

HIGHLIGHTS

- The composites of sGNS-supported vertically aligned PANI nanorods are obtained.
- The microstructure of composites can be controlled by the concentration of aniline.
- The composites with hierarchical structure show superior electrochemical performance.

GRAPHICAL ABSTRACT

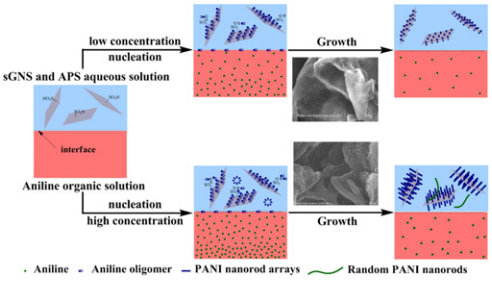

ARTICLE INFO

Article history:
Received 5 January 2012
Received in revised form
14 March 2012
Accepted 26 April 2012
Available online 8 May 2012

Keywords:
Hierarchical composites
Graphene nanosheets
Polyaniline
Interfacial polymerization
Supercapacitors

ABSTRACT

Hierarchical composites of sulfonated graphene-supported vertically aligned polyaniline nanorods (sGNS/PANI) are successfully synthesized via interfacial polymerization of aniline monomers in the presence of sulfonated graphene nanosheets (sGNS). The FE-SEM images indicate that the morphologies of sGNS/PANI composites can be controlled by adjusting the concentration of aniline monomers. FTIR and Raman spectra reveal that aligned PANI nanorod arrays for sGNS/PANI exhibit higher degree of conjugation compared with pristine PANI nanorods. The hierarchical composite based on the two-electrode cell possesses higher specific capacitance (497 F g^{-1} at 0.2 A g^{-1}), better rate capability and cycling stability (5.7% capacitance loss after 2000 cycles) than those of pristine PANI nanorods.

1. Introduction

Supercapacitors have attracted considerable attention as electrochemical energy-storage devices because of their high power density and long cycle life compared to rechargeable batteries [1–5]. To exploit advanced supercapacitors, the active electrode materials with improved performance are vital [6–9]. Polyaniline (PANI) has been regarded as one of the most promising electrode materials due to its low cost, easy and economic synthesis, high energy-storage capacity, and controllable electrical conductivity [10–12]. Unfortunately, PANI also exhibits poor cycling stability derived from the volumetric changes during the doping/dedoping process [13] and poor electrical conductivity in its neutral or alkaline state.

Ordered and aligned nanostructures should be considered to improve capacitive performance of PANI [14–18]. Nanostructured PANI can release the cycling degradation problems caused by volumetric changes or structural conformation and can provide the short diffusion path for enhanced Faradic charge transfer reactions [7].

Graphene, an intriguing two-dimensional (2-D) carbon material, is also a promising electrode material for supercapacitors due

* Corresponding author. Tel.: +86 21 64253527; fax: +86 21 64251372.
E-mail address: gengchaow@ecust.edu.cn (G. Wang).

0378-7753/$ – see front matter © 2012 Elsevier B.V. All rights reserved.
doi:10.1016/j.jpowsour.2012.04.083

to its extraordinarily high electrical conductivity and large surface area [19–21]. The combination of PANI with graphene has been proved to be another effective way to improve the capacitance and cycling stability of PANI [22–26]. However, graphene tend to form irreversible agglomeration. Moreover, both PANI and graphene are insoluble. Therefore, the uniform graphene/PANI composites cannot be obtained by conventional process methods. As a result, the functionalizations of graphene are of crucial importance. Functionalized graphenes are usually prepared by non-covalent wrapping [27–29] and covalent functionalization [30–33].

Compared with conventional graphene-based composites, the hierarchical graphene-based composites are expected to display improved performance in various applications because of excellent conducting pathways, large surface area, and high conductivity [34]. Xu et al. [35] fabricated hierarchical composites of PANI nanowire arrays on graphene oxide sheets by dilute polymerization. The hierarchical composite possessed highest specific capacitance of 555 F g^{-1} at a discharge current of 0.2 A g^{-1} and only kept 227 F g^{-1} at 2 A g^{-1}, which was ascribed to poor electrical conductivity of graphene oxide sheets. Introduction of graphene nanosheets as support of PANI arrays is highly effective to create good electrically conducting pathways. However, to our knowledge, no publications have reported the fabrication of hierarchical composites of graphene-supported aligned PANI nanorods.

In this research, we report a facile strategy to synthesize hierarchical composites of sulfonated graphene nanosheets (sGNS)-supported vertically aligned PANI nanorods (sGNS/PANI) by an interfacial polymerization method. The sGNS/PANI composites are characterized by FTIR, Raman spectroscopy, field-emission scanning electron microscopy (FE-SEM), cycle voltammetry (CV) and galvanostatic charge/discharge techniques, respectively. The resulting composites not only exhibit high electrochemical capacitance of PANI, but also keep the advantage of excellent rate performance and cycling stability of sGNS.

2. Experimental

2.1. Preparation of sulfonated graphene nanosheets

Graphite oxide (GO) was synthesized from natural graphite powder using the Hummers method [36]. The sulfonated graphene nanosheets (sGNS) were prepared following procedures described in the literature [30,33]. 0.5 g of GO was dispersed in 250 mL deionized water whose pH was adjusted to 9–10 with an ammonia solution. The GO sheets formed after 15 min sonification. The mixture was then reduced with 1.5 g of sodium borohydride at 80 °C for 1 h under constant stirring. After being centrifuged and rinsed with deionized water, the partially reduced GO was re-dispersed in 300 g of deionized water by mild sonification. The above sample was sulfonated with 0.75 g of aryl diazonium salt of sulfanilic acid in an ice bath for 2.5 h. The post-reduction with 1.9 g of hydrazine (80%) was carried out at 100 °C for 12 h to remove the remaining oxygen functional groups. The elemental analysis data of sGNS: C = 82.9%; H = 7.2%; N = 0.9%; S = 1.4%; O = 7.6% (balance).

2.2. Synthesis of sGNS/PANI composites

Hierarchical composites of sulfonated graphene nanosheets-supported vertically aligned PANI nanorods (sGNS/PANI) were synthesized by interfacial polymerization in the presence of sGNS and aniline monomer. Typical procedure was as follows: aniline monomers with various amounts (1, 2, 5, 6, 7, 8 and 10 mmol) were dissolved in 100 mL chloroform and cooled to 0 °C, respectively. sGNS (50 mg) was added into 100 mL of 1 M aqueous $HClO_4$ solution, and the mixture was sonicated for 2 h to obtain well-dispersed suspension. Then ammonium persulfate (APS) was dissolved into the above solution (the molar ratio of aniline/APS is 2) and cooled to 0 °C. The aniline solution and $HClO_4$ solution were then carefully transferred to a 500 mL beaker. The reaction was carried out at the interface of the two phases at 0 °C for 24 h. The resulting precipitates were filtered, washed with deionized water and ethanol for several times afterwards dried at 60 °C under vacuum to obtain the doped sGNS/PANI composites. For comparison, PANI nanorods were synthesized through the similar procedure above without the presence of sGNS. The weight percentage of sGNS was calculated from the weight of the composites after polymerization, thus the weight percentage and yield of PANI were also evaluated. The preparation conditions and chemical component of sGNS/PANI composites and PANI nanorods were listed in Table 1.

2.3. Characterization methods

The morphologies of the samples were examined by means of a field-emission scanning electron microscope (FE-SEM, Hitachi S-4800) and transmission electron microscopy (TEM, JEOL JEM-2100 at the accelerating voltage of 200 kV). Samples for TEM measurement were suspended in ethanol and supported on wholly carbon-coated copper grids. A Rigaku D/Max 2550 VB/PC X-ray diffractometer using the Cu-Kα radiation served as the instrument in the study of X-ray diffraction (XRD) patterns, which were recorded from 3° to 50° (2θ-angle). Fourier transform infrared spectra (FTIR) were record plotted with a Nicolet 5700 spectrometer using KBr sample pellets. Raman spectra were recorded with Renishaw inVia + Reflex using a 50 mW He–Ne laser operated at 785 nm.

2.4. Preparation of electrodes and electrochemical measurements

Electrodes were prepared by mixing 85 wt.% of carbon material, 10 wt.% of acetylene black and 5 wt.% of poly(tetrafluoroethylene) (PTFE) binder dispersed in mixed solution of deionized water and ethanol (1/1, by volume) to form a homogeneous slurry. The slurry was rolled and then pressed onto the titanium mesh. The mass of the active material mass was about 4 mg. The cell supercapacitors were composed of two symmetrical working electrodes sandwiched by a separator and the aqueous electrolyte solution of 1 M H_2SO_4.

The electrochemical performances of the cell supercapacitors were tested by cyclic voltammetry (CV) (on a CHI 760D electrochemical workstation) and galvanostatic charge–discharge tests (on an LAND CT2001A program testing system). All of the experiments were carried out in a two-electrode system. The potential

Table 1
Preparation conditions and characterization for sGNS/PANI composites and PANI nanorods.

Samples	C_{ANI} [a]	R_{wt} [b]	R_{mol} [c]	Yield of PANI (%)	Content of PANI (%)	Content of sGNS (%)
sGNS/PANI-1	0.01	1.86	2/1	16.9	23.9	76.1
sGNS/PANI-2	0.02	3.72	2/1	19.4	41.9	58.1
sGNS/PANI-3	0.05	9.3	2/1	22.9	68.0	32.0
sGNS/PANI-4	0.06	11.2	2/1	23.7	72.6	27.4
sGNS/PANI-5	0.07	13.02	2/1	26.3	77.4	22.6
sGNS/PANI-6	0.08	14.88	2/1	26.8	79.9	20.1
sGNS/PANI-7	0.1	18.6	2/1	28.1	80.9	19.1
PANI nanorods	0.07	/	2/1	22.8	100	0

[a] C_{ANI} is mole concentration of aniline.
[b] R_{wt} is aniline/sGNS weight ratio.
[c] R_{mol} is aniline/APS mole ratio.

range for CV tests was −0.2–0.8 V and the scan rate was 1 mV s^{-1}. The potential range for charge/discharge tests was −0.2–0.7 V.

2.5. Data analysis

For this two-electrode system, the specific capacitance (*Cs*) of the active electrode materials was determined by using

$$Cs = 2C/m = 2i/m(dV/dt) \quad (1)$$

in where *Cs* is specific capacitance; *i* is discharge current, *m* the mass of active electrode materials on single side, and d*V*/d*t* denotes slope of discharge curve (*V*–*t*).

The specific power (*SP*) and specific energy (*SE*) were calculated according to the following equation [1]:

$$SP = iV/m \quad (2)$$

$$SE = iVt/2m \quad (3)$$

where *i* is discharge current, *V* is the operating potential window, *m* is the mass of active material within the electrode, and *t* is discharge time.

3. Results and discussion

The FE-SEM images of PANI nanorods, and sGNS/PANI composites with various concentrations of aniline are shown in Fig. 1, respectively. As shown in Fig. 1a, the PANI prepared without the presence of sGNS shows random stacking claviform morphology with the diameter in the range of 60–80 nm. For the sGNS/PANI composites, the microstructure of composites is markedly affected by the concentration of aniline monomer. At lower concentration of aniline, the hierarchical composites of sGNS-supported vertically aligned PANI nanorod arrays are formed, and the average diameter of aligned PANI nanorods is around 10–20 nm (Fig. 1b–d). The TEM image (the inset in Fig. 1c) also exhibits the formation of arrays of homogeneous PANI nanorods (the black spots) of about 10 nm diameter. It is also found that the aligned PANI nanorods become denser with the increase of aniline concentration. However, when concentration of aniline is higher (>0.07 M), the coexisting structure of aligned PANI nanorods arrays on the sGNS and random stacking PANI nanorods with 50–80 nm diameter was formed (Fig. 1e and f).

Fig. 2 depicts the XRD patterns of sGNS, PANI nanorods and sGNS/PANI composite. The XRD pattern of sGNS has a broad peak at

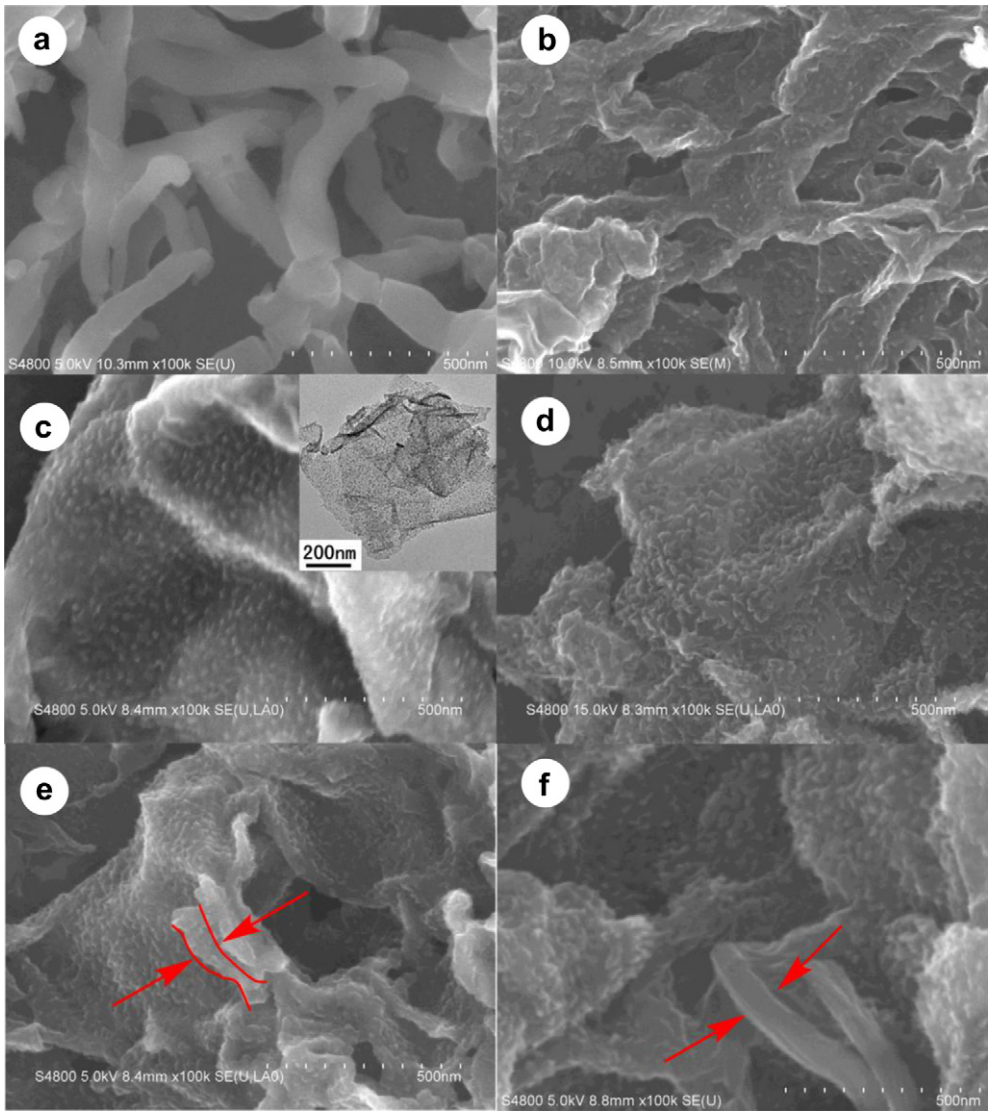

Fig. 1. FE-SEM images (a) PANI nanorods and sGNS/PANI composites with various concentrations of aniline: (b) 0.02 M, (c) 0.05 M, (d) 0.07 M, (e) 0.08 M, and (f) 0.1 M, inset in (c) showing the corresponding TEM image.

around $2\theta = 23.8^\circ$ corresponding to the diffraction of the (002) plane, which results from the irregular stack of sulfonated graphene nanosheets. Both sGNS/PANI composite and PANI nanorods exhibit two reflection peaks centered at $2\theta = 19.7$ and 24.8°, which can be ascribed to the periodicity parallel and perpendicular to PANI chains, respectively [37]. However, in the sGNS/PANI diffractogram, the peak of the periodicity perpendicular to PANI chains is obviously stronger than that of pristine PANI nanorods, which suggests that PANI nanorod arrays for sGNS/PANI have higher crystallinity compared with PANI nanorods. It can be explained that PANI nanorod arrays are vertically and orderly aligned on the surface of sGNS.

The FTIR spectra of sGNS, PANI nanorods, and sGNS/PANI composite (prepared at 0.07 M aniline) are given in Fig. 3. The spectrum of the sGNS illustrates the presence of C=C ($\nu_{C=C}$ at 1565 cm^{-1}) and $-SO_3H$ ($\nu_{S-phenyl}$ at 1170 cm^{-1}, $\nu_{O=S=O}$ at 1033 and 1003 cm^{-1}) [30,33]. The spectrum of sGNS/PANI exhibits the main IR bands similar to that of PANI nanorods. The bands at 1566, 1482, and 1291 cm^{-1} are assigned to the C=C stretching vibrations in the quinoid and benzenoid rings, and the C–N stretching vibration, respectively. It is also found that the C=C stretching vibrations of the quinoid and benzenoid rings in sGNS/PANI red-shift compared to PANI nanorods. This indicates that aligned PANI nanorod arrays exhibit higher degree of conjugation, which may results from ordered structure of PANI nanorod arrays, as well as doping effect of $-SO_3H$ groups for sGNS on PANI.

To further study the interaction between PANI and sGNS, Raman spectroscopy analysis is employed. Fig. 4 shows the Raman spectra of sGNS, PANI nanorods, sGNS/PANI composite (prepared at 0.07 M aniline). The Raman spectrum of sGNS displays a broad G band at 1603 cm^{-1} and a broad D band at 1318 cm^{-1}. For PANI nanorods, the bands appear at 1601 and 1511 cm^{-1} represent the C=C stretch of quinoid and benzenoid rings, respectively. The bands at 1376 and 1333 cm^{-1} are assigned to the C–N•$^+$ stretching. The bands at 1232 and 1175 cm^{-1} are attributed to in-plane C–H bendings of quinoid/benzenoid rings, respectively [38]. The sGNS/PANI contains the characteristic bands of both sGNS and PANI. However, compared with pristine PANI, the C=C stretch of benzenoid rings and in-plane C–H bendings of benzenoid rings in sGNS/PANI composite shift to lower wavenumbers, which also indicates the presence of π–π interaction between PANI and sGNS. This agrees with our FTIR results above.

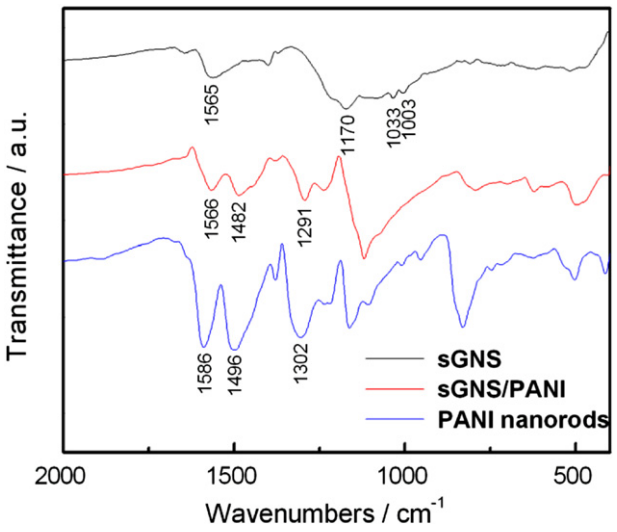

Fig. 3. FTIR spectra of sGNS, PANI nanorods, and sGNS/PANI composite prepared at 0.07 M aniline.

A formation mechanism of sGNS/PANI composites with hierarchical structure is illustrated in Scheme 1. At first, the sGNS and oxidant (APS) exist in aqueous phase and aniline monomers are dissolved in organic phase. Then the oxidative polymerization of aniline occurs and the aniline oligomers are formed at the aqueous/organic interface, and the aniline oligomers diffuse to aqueous phase. The π–π electron stacking interaction between aniline oligomers and the basal planes of sGNS leads to PANI to assemble onto the surface of the sGNS [23,35], which act the active nucleation sites of PANI growth. When aniline concentration is lower, aniline oligomers cannot achieve a supersaturation state, thus the homogeneous nucleation is suppressed. PANI nanorods further grow along the initial nuclei, consequently aligned PANI nanorods arrays on the sGNS are constructed. At higher concentration of aniline, the superfluous aniline oligomers form random stacking PANI nanorods by self-nucleation. Consequently, two morphologies of aligned PANI nanorods arrays on the sGNS and random stacking PANI nanorods are produced.

To evaluate the electrochemical performances of the supercapacitor cells based on sGNS/PANI composites, the cycle

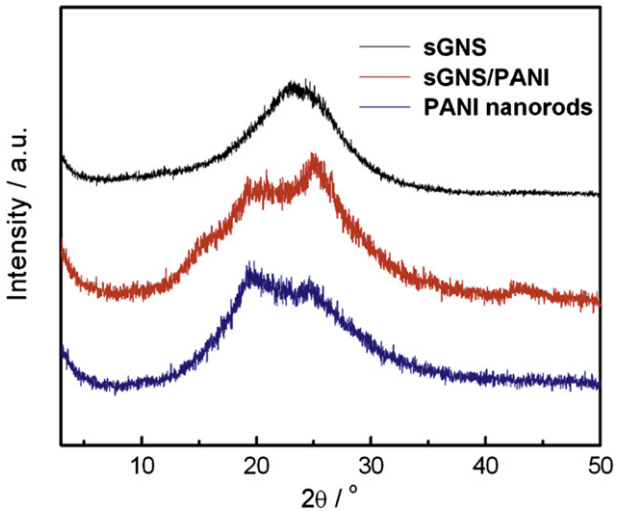

Fig. 2. XRD patterns of sGNS, PANI nanorods, and sGNS/PANI composite prepared at 0.07 M aniline.

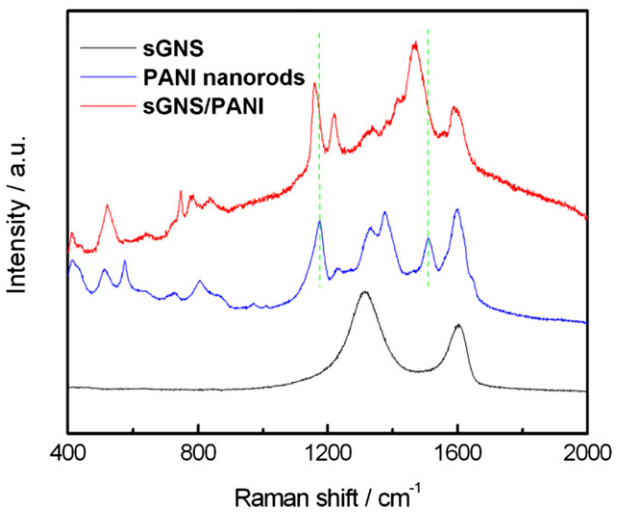

Fig. 4. Raman spectra of sGNS, PANI nanorods, and sGNS/PANI composite prepared at 0.07 M aniline.

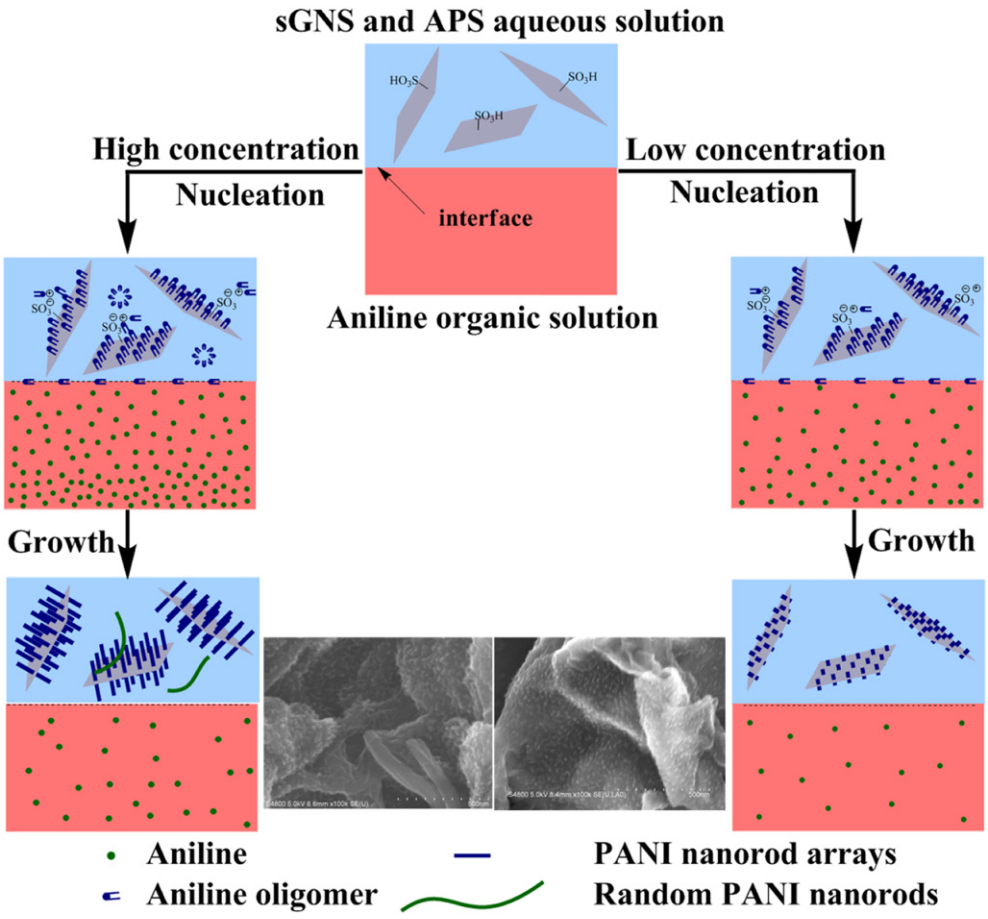

Scheme 1. Schematic presentation for fabrication of hierarchical composites of sGNS-supported aligned PANI nanorods.

voltammetry (CV) and galvanostatic charge/discharge measurements are performed in two electrode systems. Fig. 5 depicts the CVs of sGNS, pristine PANI nanorods and sGNS/PANI composite prepared at 0.07 M aniline. In both CVs of PANI nanorods and sGNS/PANI, three pairs of redox peaks are observed, which indicate that the PANI nanorods and sGNS/PANI have good pseudocapacitance characteristics. By contrast, the CV of sGNS exhibits nearly no peaks and a much smaller rectangular area.

Fig. 6 shows the charge/discharge curves of three samples at a current density of 0.2 A g^{-1}. Compared to PANI nanorods, the charge–discharge curve of sGNS/PANI shows symmetrical mirror-like image, indicating that the reversible redox reaction takes place in composite. Both pristine PANI nanorods and sGNS/PANI composite have much higher specific capacitance than that of sGNS (98 F g^{-1}). The specific capacitance of sGNS/PANI (497.3 F g^{-1}) is also much higher than the arithmetic mean of pristine PANI nanorods and sGNS ($374.4 \times 77.4\% + 98 \times 22.6\% = 311.9$ F g^{-1}) and the values of other graphene/PANI composite reported in the literature, such as graphene/PANI nanofibres (210 F g^{-1}) [24], and sulfonated graphene/PANI (356 F g^{-1}) [39], which is attributed to following two factors. First, aligned PANI nanorods have smaller dimensions (10–20 nm), which can greatly increase the utilization of PANI as an electrode material. Second, PANI nanorods vertically deposit sGNS with high conductivity, which favors the redox reaction of PANI component, thus, enhanced the pseudocapacitance of sGNS/PANI.

It is also found that the concentration of aniline has a significant influence on the specific capacitance of sGNS/PANI composites (Fig. 7). The specific capacitance of sGNS/PANI increases with the concentration of aniline from 0.01 to 0.07 M, and its value approaches maximum (497.3 F g^{-1}) at 0.07 M aniline. Afterwards, the specific capacitance goes down with the increasing concentration of aniline. This suggests that the random stacking PANI nanorods at high concentration of aniline (see Fig. 1e and f) are not adequately used during the charge/discharge process.

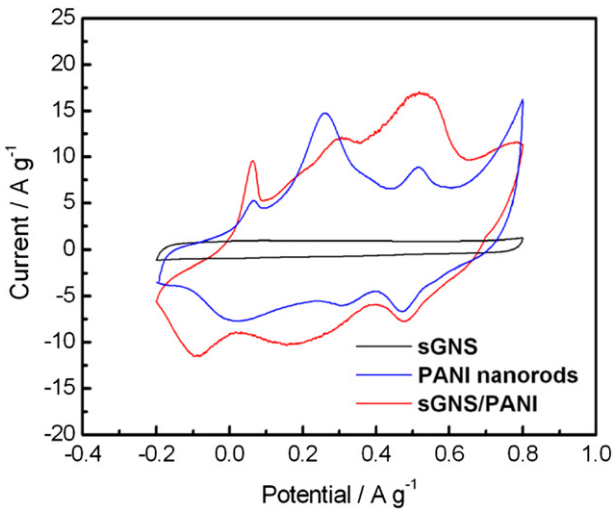

Fig. 5. CV curves at scan rate of 1 mV s^{-1} of supercapacitors based on sGNS, PANI nanorods and sGNS/PANI composite prepared at 0.07 M aniline.

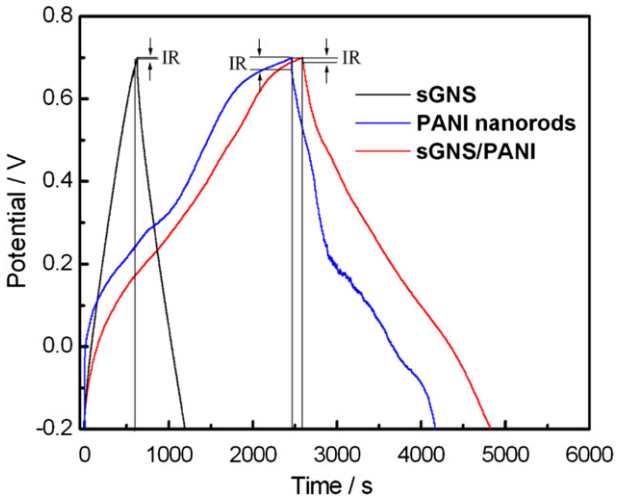

Fig. 6. Charge–discharge curves at a current density of 0.2 A $g^{-1}$of supercapacitors based on sGNS, PANI nanorods and sGNS/PANI composite prepared at 0.07 M aniline.

More importantly, the hierarchical structure with orderly arrays not only enhances the specific capacitance, but also remarkably improves the rate performance at a high current density. From Fig. 6, we can also find the IR drop of sGNS/PANI is much lower than that of pristine PANI, which reflects that the former possesses lower internal resistance compared to the latter [24,40]. Low internal resistance is beneficial to the improvement of rate performance in supercapacitors. As shown in Fig. 8a, the composite kept 67.6% of its capacitance (497.3–336.3 F g^{-1}) as current density is increased from 0.2 to 10 A g^{-1}, while the PANI nanorods lost 67.4% (374.4–122.2 F g^{-1}) of its capacity in the same condition. This rate capability is significantly superior to the result reported for the composite of PANI nanowire arrays on GO sheets in the literature [35]. The excellent rate performance is ascribed to the high conductivity of sGNS as a support hastened charge transport and the hierarchical structure with orderly arrays of PANI nanorods benefited ionic transfer. The Ragone plots of PANI nanorods and sGNS/PANI also reveal that the sGNS/PANI has high power capability. As shown in Fig. 8b, sGNS/PANI composite delivers a high energy density of 41.5 Wh kg^{-1} at a power density of 4.5 kW kg^{-1}, which is about 2.8 times larger than that of pristine PANI nanorods.

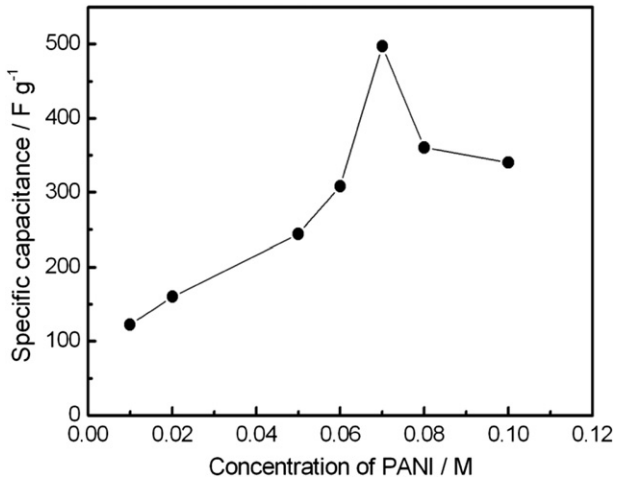

Fig. 7. Influence of aniline concentration on specific capacitance of sGNS/PANI composites.

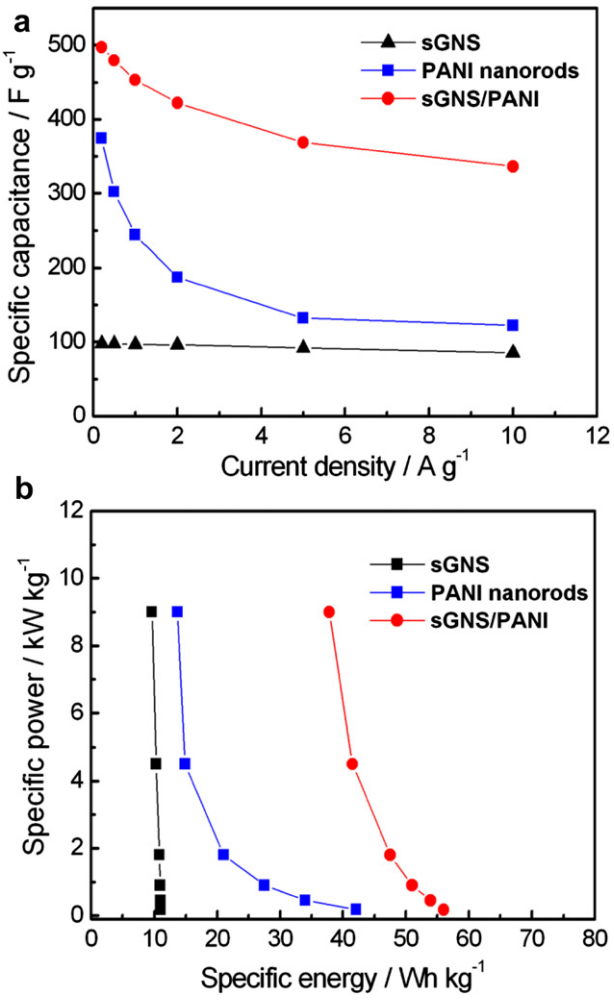

Fig. 8. (a) The specific capacitance as a function of various current densities; (b) Ragone plots (specific power vs. specific energy) of sGNS, PANI nanorods, and sGNS/PANI composite prepared at 0.07 M aniline.

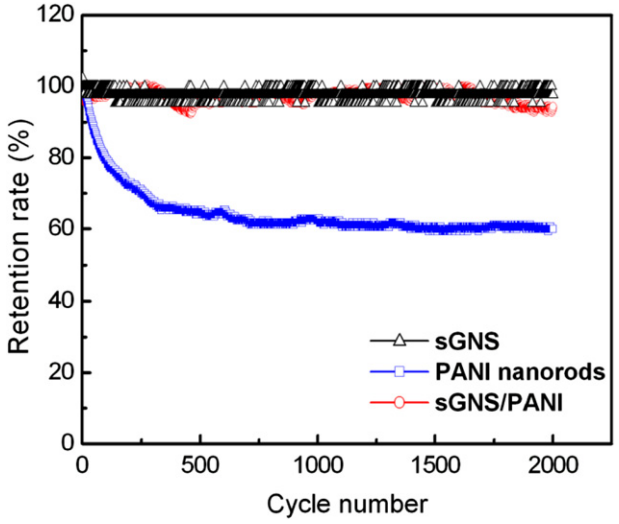

Fig. 9. Cycling stability at a current density of 1 A g^{-1} of supercapacitors based on sGNS, PANI nanorods and sGNS/PANI composite prepared at 0.07 M aniline.

The stability of PANI nanorods and sGNS/PANI is examined by charge/discharge cycles at a current density of 1 A g^{-1} for 2000 cycles (Fig. 9). The capacitance retention of the composite still maintains 94.3% of its initial capacitance, while pure PANI nanorods kept only 60% of its initial capacity. The better stability of sGNS/PANI is possibly attributed to the use of sGNS with exceptional mechanical properties as a support and the π–π interaction between aligned PANI nanorods and the basal planes of sGNS.

4. Conclusions

In this paper, an interfacial polymerization method that synthesizes hierarchical composites of sGNS-supported vertically aligned PANI nanorods (sGNS/PANI) is developed. The hierarchical structure with orderly arrays for sGNS/PANI leads to significantly enhanced electrochemical capacitance (497.3 F g^{-1}), rate performance and cycling stability (94.3% capacitance retention after 2000 cycles) compared to pure PANI nanorods. The results suggest that the hierarchical composites are very promising candidates for supercapacitor materials.

Acknowledgements

We greatly appreciate the financial supports of National Natural Science Foundation of China (21044005, 51173042), Fundamental Research Funds for the Central Universities, Innovation Program of Shanghai Municipal Education Commission (11ZZ55) and Shanghai Key Laboratory Project (08DZ2230500).

References

[1] B.E. Conway, Electrochemical Supercapacitors, Scientific Fundamentals and Technological Applications, Kluwer Academic/Plenum Press, New York, 1999.
[2] P. Simon, Y. Gogotsi, Nat. Mater. 7 (2008) 845–854.
[3] H. Liu, L.-H. Jin, P. He, C. Wang, Y.-Y. Xia, Chem. Commun. (2009) 6813–6815.
[4] L.-L. Zhang, X.-S. Zhao, Chem. Soc. Rev. 38 (2009) 2520–2531.
[5] F.-L. Zheng, G.-R. Li, Y.-N. Ou, Z.-L. Wang, C.-Y. Su, Y.-X. Tong, Chem. Commun. 46 (2010) 5021–5023.
[6] G.-W. Yang, C.-L. Xu, H.-L. Li, Chem. Commun. (2008) 6537–6539.
[7] Y. Wang, H. Li, Y.-Y. Xia, Adv. Mater. 18 (2006) 2619–2623.
[8] L.-Z. Fan, Y.-S. Hu, J. Maier, P. Adelhelm, B. Smarsly, M. Antonietti, Adv. Funct. Mater. 17 (2007) 3083–3087.
[9] H. Jiang, T. Zhao, J. Ma, C.-Y. Yan, C.-Z. Li, Chem. Commun. 47 (2011) 1264–1266.
[10] D. Li, J.X. Huang, R.B. Kaner, Acc. Chem. Res. 42 (2009) 135–145.
[11] K.S. Ryu, K.M. Kim, N.G. Park, Y.J. Park, S.H. Chang, J. Power Sources 103 (2002) 305–309.
[12] P. Novak, K. Muller, K.S.V. Santhanam, O. Hass, Chem. Rev. 97 (1997) 207–281.
[13] E. Frackowiak, V. Khomenko, K. Jurewicz, K. Lota, F. Béguin, J. Power Sources 153 (2006) 413–418.
[14] V. Gupta, N. Miura, Electrochem. Solid-State Lett. 8 (2005) A630–A632.
[15] B.K. Kuila, B. Nandan, M. Bëhme, A. Janke, M. Stamm, Chem. Commun. (2009) 5749–5751.
[16] X.-M. Zhu, L.-Q. Wang, J.-P. Lin, L.-S. Zhang, ACS Nano 9 (2010) 4979–4988.
[17] K. Wang, J.-Y. Huang, Z.-X. Wei, J. Phys. Chem. C 114 (2010) 8062–8067.
[18] Y.-F. Yan, Q.-L. Cheng, G.-C. Wang, C.-Z. Li, J. Power Sources 196 (2011) 7835–7840.
[19] M.D. Stoller, S. Park, Y. Zhu, J. An, R.S. Ruoff, Nano Lett. 8 (2008) 3498–3502.
[20] Y. Wang, Z.-Q. Shi, Y. Huang, Y.-F. Ma, C.-Y. Wang, M.-M. Chen, Y.-S. Chen, J. Phys. Chem. C 113 (2009) 13103–13107.
[21] J.R. Miller, R.A. Outlaw, B.C. Holloway, Science 329 (2010) 1637–1639.
[22] D.-W. Wang, F. Li, J.-P. Zhao, W.-C. Ren, Z.-G. Chen, J. Tan, Z.-S. Wu, I. Gentle, G.-Q. Lu, H.-M. Cheng, ACS Nano 3 (2009) 1745–1752.
[23] J. Yan, T. Wei, B. Shao, Z.-J. Fan, W.-Z. Qian, M.-L. Zhang, F. Wei, Carbon 48 (2010) 487–493.
[24] Q. Wu, Y.-X. Xu, Z.-Y. Yao, A.-R. Liu, G.-Q. Shi, ACS Nano 4 (2010) 1963–1970.
[25] H.-L. Wang, Q.-L. Hao, X.-J. Yang, L.-D. Lu, Xin Wang, Nanoscale 2 (2010) 2164–2170.
[26] K. Zhang, L.-L. Zhang, X.S. Zhao, J.-S. Wu, Chem. Mater. 22 (2010) 1392–1401.
[27] S. Stankovich, R.D. Piner, X.Q. Chen, N.Q. Wu, S.T. Nguyen, R.S. Ruoff, J. Mater. Chem. 16 (2006) 155–158.
[28] Y. Xu, H. Bai, G. Lu, C. Li, G. Shi, J. Am. Chem. Soc. 130 (2008) 5856–5857.
[29] H. Bai, Y. Xu, L. Zhao, C. Li, G. Shi, Chem. Commun. (2009) 1667–1669.
[30] Y. Si, E.T. Samulski, Nano Lett. 8 (2008) 1679–1682.
[31] Z. Liu, J.T. Robinson, X.M. Sun, H.J. Dai, J. Am. Chem. Soc. 130 (2008) 10876–10877.
[32] J.F. Shen, Y.Z. Hu, C. Li, C. Qin, M.X. Ye, Small 5 (2009) 82–85.
[33] L.-F. Jin, G.-C. Wang, X.-W. Li, L.-B. Li, J. Appl. Electrochem. 41 (2010) 377–382.
[34] Z.-J. Fan, J. Yan, L.-J. Zhi, Q. Zhang, T. Wei, J. Feng, M.-L. Zhang, W.-Z. Qian, F. Wei, Adv. Mater. 22 (2010) 3723–3728.
[35] J.-J. Xu, K. Wang, S.-Z. Zu, B.-H. Han, Z.-X. Wei, ACS Nano 4 (2010) 5019–5026.
[36] W.S. Hummers, R.E. Offeman, J. Am. Chem. Soc. 80 (1958) 1339.
[37] J.P. Pouget, M.E. JTzefowicz, A.J. Epstein, X. Tang, A.G. MacDiarmid, Macromolecules 24 (1991) 779–789.
[38] M. Cochet, G. Louarn, S. Quillard, J.P. Buisson, S. Lefrant, J. Raman Spectrosc. 31 (2000) 1041–1049.
[39] Q.L. Hao, H.L. Wang, X.J. Yang, L.D. Lu, X. Wang, Nano Res. 4 (2011) 323–333.
[40] G.H. Yu, L.B. Hu, M. Vosgueritchian, H.L. Wang, X. Xie, J.R. McDonough, X. Cui, Y. Cui, Z.N. Bao, Nano Lett. 11 (2011) 2905–2911.